Physica A 616 (2023) 128623

Contents lists available at ScienceDirect

Physica A

journal homepage: www.elsevier.com/locate/physa

# Simultaneous improvement of multiple transportation performances on link-coupled networks by global dynamic routing

Chao Yang [a], Zhuoran Chen [a], Jianghai Qian [b,*], Dingding Han [a,c,*], Kaidi Zhao [a]

[a] School of Information Science and Technology, Fudan University, Shanghai, 200233, China
[b] School of Mathematics and Physics, Shanghai University of Electric Power, Shanghai, 201306, China
[c] Shanghai Artificial Intelligence Laboratory, Shanghai, 200232, China

ARTICLE INFO

*Article history:*
Received 1 December 2022
Received in revised form 24 January 2023
Available online 1 March 2023

*Keywords:*
Complex network
Routing algorithm
Global dynamic routing
Braess paradox
Transportation dynamics
Routing

ABSTRACT

The interconnected networks are facing with critical congestion issue due to the rapid growth of the traffic and the information on the links with limited capacity. We show that the traditional routing strategies are generally confronted with a tradeoff between the network capacity and the link usage when applying to the link-coupled network. To take a step to the issue, we propose a global dynamic routing (GDR) strategy that can simultaneously achieve multiple improvement of the transport performance with acceptable computational complexity at the cost of the average arrival time. Further analysis indicates the improvement is related to the nontrivial load distribution resulting from GDR. More surprisingly, the simulation experiments suggest our strategy GDR can suppress the occurrence of Braess-like paradox, which is a long-standing problem in transportation.



## 1. Introduction

The development of the Cyber–Physical Systems are promoting multiple systems, such as communication networks, transportation network and power network, to get highly engaged with each other [1–10]. A possible consequence brought by this kind of interconnected system is that the information from different subsystems will transport on a single coupled link, causing a rapid growth of the traffic and exacerbating the consumption of the resources such as bandwidth. This new situation challenge the most existing routing strategies [11–16] that typically focus on nodes capacity and might result in serious congestion problems [17–23].

In link-coupled networks, different subsystems share common links to deliver messages and traffic flow. On the communication network, due to the high cost of laying special lines, a new communication link often attaches partially to couples with an existing communication network [24]. On the transportation network, some cities use the bridging services temporarily substituting segments of the subway network for better performance on the significant backbones, sucn as the intermodal bus-and-train transit network [25,26]. On the Internet, more than two nodes can share the same IP link if the nodes are all connected to the same layer 2 switch (Asynchronous Transfer Mode, Ethernet, etc.) [27]. When applying the routing strategy designing for node-coupled networks or single network systems directly to link-coupled networks, we notice that the performance of the network capacity and the link usage usually gets their respective

* Corresponding authors.
*E-mail addresses:* qianjianghai@shiep.edu.cn (J. Qian), ddhan@fudan.edu.cn (D. Han).

https://doi.org/10.1016/j.physa.2023.128623
0378-4371/

improvement at the cost of the other. In specific, routing based on global strategies such as short path strategy that prefers high betweenness links leads to low transmission resources utilization, while those adopting local strategies that utilize neighbor information suffers from useless transmissions. Such tradeoff indicates a bottleneck and limitations of the existing routing strategy, which hampers the improvement of the interconnected systems.

We propose a global dynamic routing strategy (GDR) based on the coupling characteristics to fill the mentioned gap. GDR uses global dynamic information to find the shortest node queue and utilizes dynamic information of coupled links to reduce the adverse effect of other layers. It is worth noting that literature [28] considers the intra-layer global dynamic information, but does not consider the effect among different layers of the multi-layer network. The coupling of different layers is also an important factor affecting network transmission. The high-priority networks delay the transmission of low-priority networks in the link-coupled networks. The transmission speed of different layers also greatly affects the efficiency [29]. The GDR takes into account two types of factors. We study network capacity, link usage, average arrival time ($AAT$), and steady-state load distribution during the transmission process on the link-coupled networks. GDR simultaneously achieves a variety of transportation performance improvements, especially network capacity and link usage. By introducing the time delay $\delta t$, GDR sacrifices an acceptable $AAT$ in exchange for a great improvement in time complexity without affecting the network capacity and link usage. Further analysis shows that GDR presents a load distribution like local strategies, which is the key to resolving the tradeoff and achieving better performance. Using inter-layer coupled dynamic information, GDR achieves shorter $AAT$s at low-priority layers. Furthermore, our work provides a preliminary attempt at widespread Braess's paradox [30–36]. The results show that the existing routing strategies lead to the Braess's paradox and the serious congestion when adding a new transmission link. However, GDR suppresses the occurrence of Braess-like paradox to a certain extent. We also give an example of congestion without inter-layer coupled dynamic information in our experiments.

The rest of the paper is organized as follows. Section 2 describes the link-coupled network model and the GDR strategy. Section 3 shows the results of perfomance indicators on the link-coupled network, followed by a analysis of load distribution in Section 4 and the experimental results of Braess's paradox are in Section 5. Section 6 summarizes this paper.

## 2. Network model and routing strategy

### 2.1. Link-coupled networks

The link-coupled network is a $l$-layer network. Each layer has a certain number of links coupled with the links on other layers to share the bandwidth, thus called link-coupled network. Those nodes of the coupled links are coupled nodes. Nodes and edges in layer $L_i$ are expressed as $n_i$ and $e_i$, $i \in [1, l]$. The details of the example network are shown in Fig. 1(a).

At each step, $R$ packets are generated in each layer, delivered along a given path according to the first-in–first-out (FIFO) rule and removed when reaching its destination. The packets are stored in the buffer queue of nodes. The origin and the destination of each packet are chosen randomly and the route is given by routing strategy. We assume a link only forwards one packet in a time step and layer with small $i$ has higher priority. When packets on different layers pass through the same link at the same time, the transmission order is determined by the priority of the layer. Fig. 1(b)–(f) show an example of transmission process. When packets in $L_1$ and $L_2$ arrive at both ends of the coupled link and use the same link simultaneously, the packet in $L_1$ has higher priority and occupies the link, while the packet in $L_2$ waits until the coupled link is not occupied.

### 2.2. Global dynamic routing

GDR takes the path with the shortest dynamic distance. The dynamic distance $L_{od}$ from origin ($o$) to destination ($d$) is defined as:

$$L_{od} = \sum_{m=o}^{d} \left[ 1 + \sum_{k} n_m^k \right] \tag{1}$$

where the first term is the hop count from $o$ to $d$, $n_m^k$ is the buffer queue length of node $x_m$ in layer $L_k$. If the node $x_m^k$ has coupled nodes at other layers, $\sum_k n_m^k$ sums the queue lengths of those coupled nodes on other layers. Otherwise, $\sum_k n_m^k$ only calculates the queue length of this layer. The queue length of all layers of the link-coupled network is first obtained in the iteration, and the shortest path is calculated for each new packet based on Eq. (1) later. It is worth noting that the length of node queue and dynamic distance vary with time. The shortest path of the new packet may also be different. Therefore, the routing path of all packets on the network needs to be calculated in real time.

GDR utilizes both intra-layer global and inter-layer coupled dynamic information for navigation. The intra-layer global dynamic information includes the network topology and the buffer queue lengths. The inter-layer coupled dynamic information includes the coupled links structure and the buffer queue lengths of the corresponding nodes. $L_{od}$ realizes the optimization of two aspects, which corresponds to the utilization of the above two types of dynamic information. One

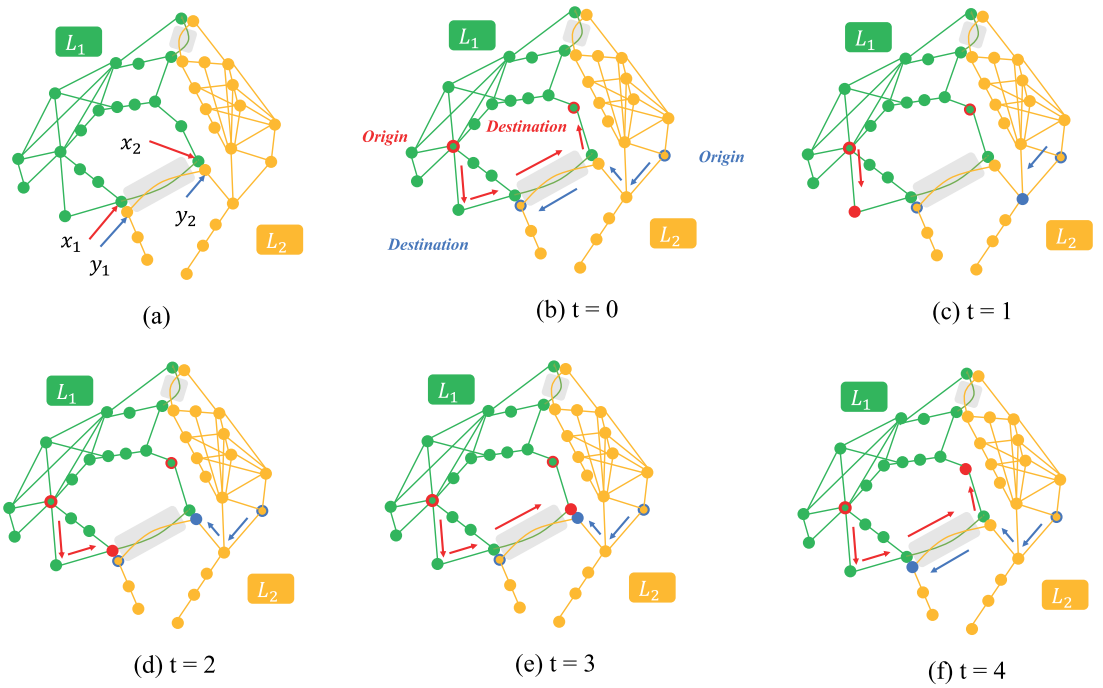


**Fig. 1.** Link-coupled network illustration. (a) $L_1$ and $L_2$ are coupled by the gray links. $L_1$ has a higher priority. $x_1$ and $y_1$ are coupled nodes, So are $x_2$ and $y_2$. (b) $t = 0$. Two packets start in $L_1$ and $L_2$ respectively from origins at the same time. (c) $t = 1$. Two packets go separately and do not affect each other. (d) $t = 2$. Two packets reach the ends of the coupled link at the same time. (e) $t = 3$. The packet in $L_1$ has higher priority and occupies the coupled link for transmission, while the packet in $L_2$ waits. (f) $t = 4$. The packet in $L_2$ reaches its destination through the coupled link. The packet in $L_1$ also reaches its destination.

is the intra-layer optimization. The newly generated packets are routed to the path with more hops but fewer packets, so as to realize the full utilization of transmission resources. The other one is the inter-layer optimization. The queue length of coupled nodes is treated as the queue length of this layer, which makes $L_{od}$ larger, thus reducing the use of coupled links and reducing the performance loss of low-priority networks.

## 3. Experiment results

### 3.1. Parameters setting

Each layer of the experiment two-layer link-coupled network is a scale-free network with $N = 500$ nodes and degree distribution exponent $\gamma = 3$. There are $\beta|e_1|$ random coupled links in the two-layer network, where $\beta \in [0, 1]$ is the coupled strength between two layers and $|e_1|$ is the number of edges in layer 1. We compare GDR with shortest path (SP), effective routing (ER) [11] and integrating local static, dynamic information routing (ILSDI) [15] strategies and single layer global routing strategies(SGR) [28] on scale-free networks.

### 3.2. Capacity and link usage

Order parameter [37] describes the congestion of the interconnected system, which is defined as:

$$H(R) = \lim_{t\to\infty} \frac{A}{R} \frac{\langle \Delta W \rangle}{\Delta t} \tag{2}$$

where $R$ is the packets number added in each step, $A$ is the parameter that equals to the average degree $\langle k \rangle$ to represents average transmission capacity of each node, and $\Delta W = W(t+\Delta t) - W(t)$, where $W(t)$ represents total number of packets in the system at time $t$.

$H(R)$ is the ratio of packets generated to packets arrived at each time step. When $H(R) = 0$, the generated packets and the arrived packets are in equilibrium, and packets can be transferred to their destination in time. The total number of loads on the system remains constant, and the system reaches a steady state finally. With the increase of $R$, the packets generated in each time step could not be transmitted in time limited by the link capacity. Gradually, the packets accumulate and the network is congested when $H(R) > 0$. The system emerges a phase transition from a free-flow state to a congested state at the critical value $R_c$ denoted as traffic capacity.

**Table 1**
The comparison of critical link usage $\mu_c$ with different strategies.

| | GDR | SP | ER | ILSDI | SGR |
|---|---|---|---|---|---|
| $\mu_c$ | 1.138 | 0.039 | 0.374 | 0.535 | 1.094 |

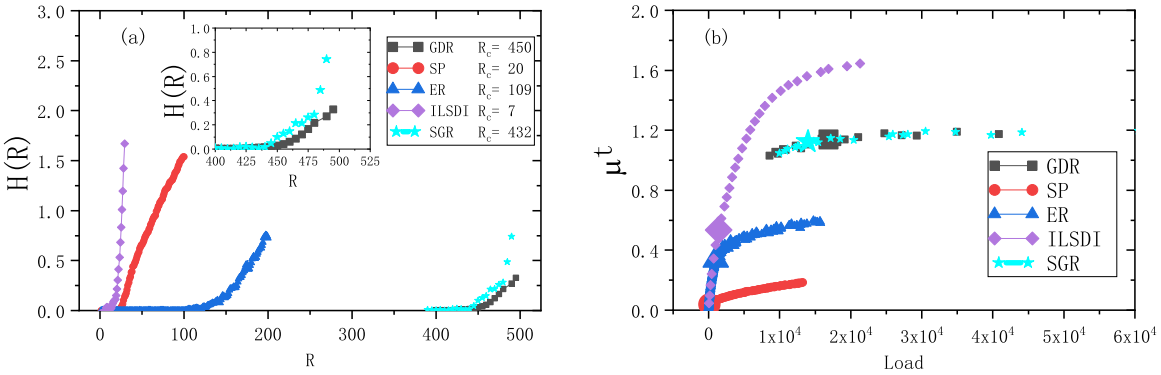


**Fig. 2.** Simulation results of network capacity and link usage. The simulation results when $l = 2$ and $\beta = 0.1$. With a given $R$, the network reaches a steady state finally. (a) The relationship between the order parameter $H(R)$ and $R$. A phase transition emerges with the increase of $R$, and the $R$ value at phase transition is the traffic capacity $R_c$ of the strategy. GDR achieves the highest traffic capacity among all strategies. Inset: The enlarged display of $R \in [400, 500]$. The phase transition point of SGR is slightly lower than that of GDR. (b) The relationship between the link usage $\mu_t$ and the load (the total number of FIFO queue for all nodes) in the steady-state system. $R_c$ are marked with larger symbols.

Link usage is defined as the proportion of occupied links as

$$\mu^t = \frac{\sum_l \left|\widehat{e_i^t}\right|}{\sum_l |e_i|} \tag{3}$$

where $\left|\widehat{e_i^t}\right|$ is the number of occupied links in $L_i$ at time step $t$, $|e_i|$ is the number of links of $L_i$, and $\mu^t$ is usage rate of the link at time step $t$.

Fig. 2 shows the simulation results of network capacity and the link usage with $l = 2$ and $\beta = 0.1$. The link usage and load of the points in Fig. 2(a) and (b) correspond to each other. Fig. 2(a) shows the phase transition of $H(R)$. GDR has the highest network capacity among all strategies. Fig. 2(b) shows the phase transition of $\mu_t$. When $R < R_c$, $\mu_t$ increases with the load and the system becomes stable finally. When $R > R_c$, the system cannot reach steady state and the load keeps increasing with time. In this case, $\mu_t$ and load in Fig. 2(b) take the quantity of corresponding time step. Since the usage is highly related to $R$, we further study the critical link usage $\mu_c$, that is, the $\mu$ when $R = R_c$. We find the $\mu_c$ of GDR strategy at steady-state is the highest as shown in Table 1. The performance of GDR is a little better than that of SGR, which means that our improvements of inter-layer coupled dynamic information is beneficial. The characteristics of the strategies are different on the link-coupled network. Routing based on global strategies such as short path strategy that prefers high betweenness links leads to low transmission resources utilization, while those adopting local strategies that utilize neighbor information suffers from useless transmissions and low network capacity. It demonstrates a tradeoff phenomenon between global and local strategies in terms of network capacity and link usage. However, GDR can achieve the high network capacity and link usage on link-coupled networks simultaneously.

When the coupled strength $\beta$ increases, high-priority layers occupy more coupled link, and the performance of low-priority layers degrade. Fig. 3(a) and (b) shows the traffic capacity and link usage with different coupled strengths. With the increase of $\beta$, the number of coupled links increases, and more bandwidth in $L_2$ are occupied by $L_1$. The overall network performance decreases gradually. Fig. 3(c) shows the total number of packets in each layer with time step when $R = 1.1R_c$. The load of $L_1$ keeps stable while that of $L_2$ increases. The transmission process at higher-priority layer $L_1$ is not affected, while $L_2$ is congested gradually and the phase transition of the whole network emerges since the bandwidth of the coupled links in $L_2$ is occupied by the packets in $L_1$.

### 3.3. Average arrival time

The average arrival time ($AAT$) is the average time step required by a packet transmission (from the origin to the destination including the waiting time). The smaller $AAT$ is, the faster the package reaches their destinations. The simulation result of $AAT$ is shown in Table 2. Compared with local strategy ILSDI, GDR delivers more packets (81 times) in less time. Compared with global strategies including SP and ER, GDR trades an acceptable $AAT$ for a larger improvement in traffic capacity.

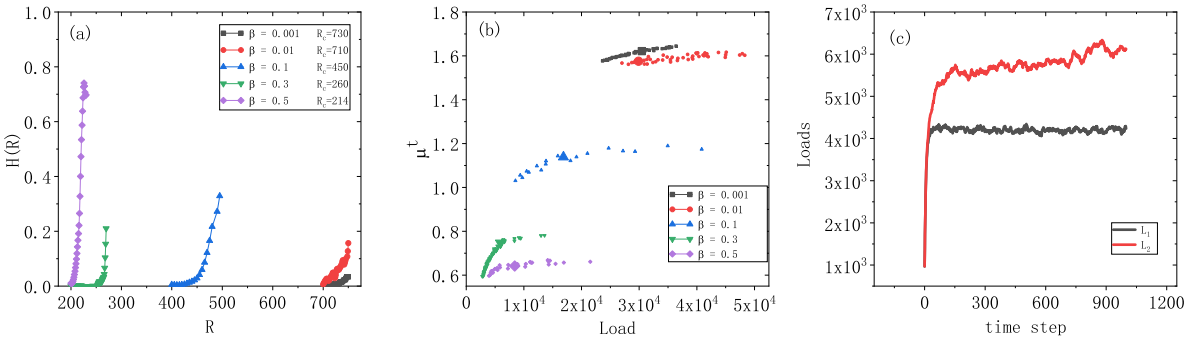


**Fig. 3.** Comparison of network transportation performances with different coupled strengths. (a) The trend between order parameter $H(R)$ and $R$ with different coupled strengths $\beta$; (b) The trend between link usage $\mu^t$ and load with different coupled strengths $\beta$; (c) The number of loads at different layers increases with time step when $\beta = 0.1$ and $R = 1.1R_c$.

**Table 2**
The comparison of *AAT* with different strategies when $\beta = 0.1$ and $R = 0.9R_c$.

| Strategies | GDR | SP | ER | ILSDI | SGR |
|---|---|---|---|---|---|
| $R = 0.9R_c$ | 405 | 18 | 98 | 6 | 388 |
| $L_1$ AAT | 11.148 | 3.022 | 4.717 | 68.903 | 9.523 |
| $L_2$ AAT | 10.816 | 3.006 | 5.408 | 70.717 | 11.183 |

As mentioned in Section 3.2, due to the priority of link-coupled networks, lower-priority $L_2$ is affected by $L_1$. The *AAT* of $L_2$ is higher than that of $L_1$. To reduce the impact of inter-layer priority, we introduce inter-layer dynamics into GDR as shown in Eq. (1). Taking the queue lengths of coupled nodes in other layers as that in this layer, $L_2$ avoids the effect of $L_1$ and reduces the performance degradation caused by coupled links. The *AAT* of $L_2$ avoids the effect of $L_1$ only in GDR and SP according to Table 2. In particular, SP performs poorly in disassortative coupled model [24], while GDR is not limited by the coupled model.

Overall, GDR has the best transportation performance and overcomes the performance degradation of low-priority layer affected by coupled links.

### 3.4. Time delay influences and time complexity

The calculation of GDR is equivalent to the weighted Dijkstra algorithm, and its time complexity is $O(Nlog(N))$. The shortest dynamic distance and $n_m^k$ vary with iteration time. Therefore, the routing table needs to be recalculated when new packets are added at each time step. If the routing table can be cached and updated periodically, the computational complexity can be reduced. We introduce time delay $\delta t$ to reduce the time complexity based on the above idea. When $t = n\delta t$ $(n \in N^*, \delta t \in N^*)$, GDR repeatedly calculates the routing path and updates corresponding routing table. When $t \in (n\delta t, (n+1)\delta t)$, GDR keeps the routing table of last step. Thus the average time complexity is reduced to $O(Nlog(N)/\delta t)$.

The results of different $\delta t$ are shown in Fig. 4. The network reaches the steady state with $R = R_c$ regardless of the value of $\delta t$ as shown in Fig. 4(a). The link usage of the network is not affected by $\delta t$ as shown in Fig. 4(b). The load distribution of GDR in steady state is approximately Poisson distribution, but the mean and variance increase with the $\delta t$ as shown in Fig. 4(c). *AAT* increases linearly with $\delta t$ as shown in Fig. 4(d).

We observe a step-up phenomenon in link usage and a subsequent slow decrease, as shown in Fig. 4(b). This step-up occurs when $t = \delta t$. This phenomenon indicates that the renewal of routing table leads to a higher link usage of the network since GDR guides newly generated packets to links with lower link usage.

To sum up, the system reaches steady state with $R = R_c$ regardless of the value of $\delta t$. The network capacity, link usage and load distribution in steady state remain unchanged. However, the time steps and *AAT* to reach the steady state increases with the increase of $\delta t$. GDR trades a certain *AAT* for an increase in time complexity.

## 4. Load distributions

A tradeoff between network capacity and link usage occurs when existing routing strategies are applied to the link-coupled network. The design of local strategies results in a more balanced load distribution, while global strategies may lead to congestion at certain critical nodes, resulting in an unbalanced load distribution [11,16]. This conclusion is also verified by Fig. 5.

As shown in Fig. 5(a), the steady state distribution of local strategies(ILSDI) resembles a Poisson distribution. Its peak occurs in the middle, with low frequencies at the ends. In Fig. 5(b)(SP) and (c)(ER) the steady state distribution of global

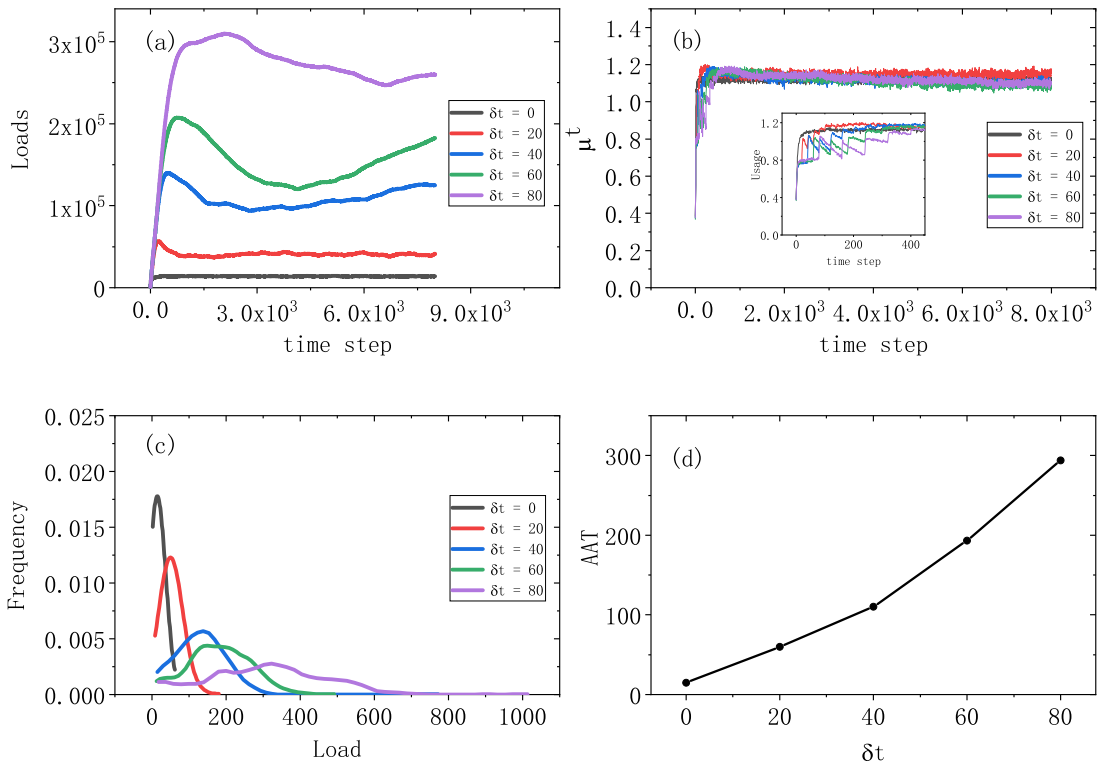


**Fig. 4.** The comparison of transmission state with different time delay $\delta t$ when $R = R_c$. (a) The trend of system load. (b) The trend of link usage. Inset: The enlarged display of time step $\in [0, 400]$. (c) The load distribution of each node in the system when $t = t_{sample}$. (d) The trend between average arrival time $AAT$ and $\delta t$.

strategies is similar to a power-law distribution, where a small number of nodes have higher loads. The approximate Poisson distribution has higher link usage than the approximate power-law distribution according to rank result in Appendix A. The Appendix A gives the reason for obtaining the sampling time and the rank of the link usage in steady state. SGR presents an approximate Poisson distribution trend, but there is still a peak on the left side of the distribution. Unexpectedly, GDR which is a global strategy has similar distribution characteristics as the local strategies. GDR allows packets to be delivered on lower-loaded paths, thus achieving an approximate Poisson distribution in steady state. This phenomenon also explains the higher network capacity of GDR at the micro level.

Next we further analyze the relationship between load distribution and network capacity. In order to calculate the network capacity $R_c$, we have firstly defined the edge betweenness with different node weights in Eq. (4), where $e_i^j$ is an edge in the set $e_i$, $g_i(e_i^j, w)$ represents the edge betweenness of $e_i^j$ with node weight $w$, $\sigma^{od}(e_i^j, w)$ is the number of shortest paths pass edge $e_i^j$ and $\sigma^{od}(w)$ is the number of shortest paths between nodes $o$ and $d$.

$$g_i(e_i^j, w) = \sum_{o \neq d} \frac{\sigma^{od}(e_i^j, w)}{\sigma^{od}(w)} \tag{4}$$

The larger betweenness is, the more packets will be navigated to this edge with this strategy, and the greater the probability of congestion is. Therefore, the steady-state load distribution is actually a representation of the betweenness. In each time step, $R$ packets are generated at each layer, so the average number of packets passing edge $e_i^j$ is Eq. (5).

$$\langle \Theta \rangle = R \frac{g_i(e_i^j, w)}{|n_i|\,(|n_i| - 1)} \tag{5}$$

When $R \leq R_c$, the packet can be sent to the destination in time. There is no packet accumulation on any edge. In other words, $\langle \Theta \rangle < 1$. When $\langle \Theta \rangle > 1$, the congestion occurs. Therefore, the phase transition occurs when the $\langle \Theta \rangle$ of edge with maximum betweenness is equal to 1. The critical packet generating number $R_c$ should fulfill Eq. (6).

$$R_c = \frac{|n_i|\,(|n_i| - 1)}{\max g_l\left(e_l^j, w\right)} \tag{6}$$

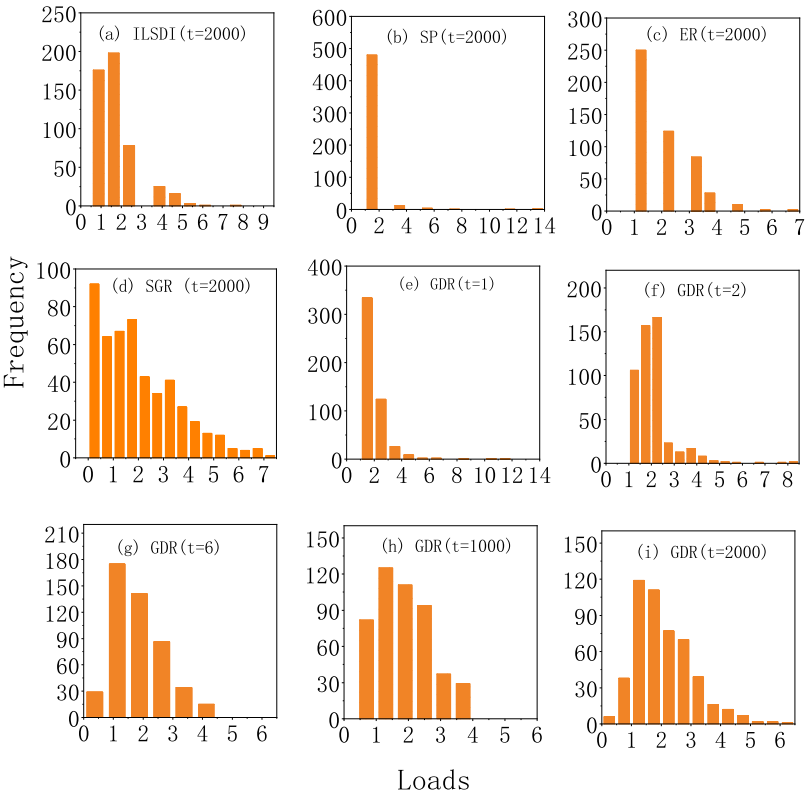


**Fig. 5.** Load distributions with different strategies. We set $R = 0.9R_c$. $t$ is the simulation time step and $t_{sample}$ is the number of sampled simulation time step when the system reaches the steady state. We set $t_{sample} = 2000$ according to Appendix A. All distribution diagrams have been normalized, subtracting the mean and dividing by the variance. Panels (a)–(d) show the simulation load distribution of ILSDI, SP, ER and SGR. Panels (e)–(i) show the load distributions of GDR with $t = 1, 2, 3, 6, 1000, t_{sample}$.

**Table 3**
The specific value of $\max g_2(e, w)$ with different strategies.

| Strategies | ER | GDR | SP |
|---|---|---|---|
| $\max g_2(e, w)$ | 0.00889 | 0.00848 | 0.03 |

It is worth noting that in the link-coupled networks, according to the conclusion in Section 3.2, the network capacity depends on the network capacity of the low-priority network, thus $\max g_i(e_i^j, w) = \max g_l(e_l^j, w)$. The results show $R_c \propto \frac{1}{\max g_l(e_l^j, w)}$ The shortest path and $\max g_l(e_l^j, w)$ is calculated in different ways with different global routing strategies. Different strategies have different node weights. The node weight is 1 in SP, the power of the node degree in ER, and the node queue length in GDR, respectively. It is difficult to calculate the theoretical value of $\max g_l(e_l^j, w)$. We use the above experimental data to calculate the $\max g_2(e, w)$. The specific values are shown in the Table 3. The $\max g_2(e, w)$ of GDR is the smallest, which indicates that the network capacity of GDR is the largest.

When the total number of loads is fixed, if the load distribution is more evenly, the $\max g_l(e_l^j, w)$ is smaller and the network capacity is larger, which explains the relationship between the load distribution and the network capacity.

Fig. 5 (e)–(i) show the dynamics of load distributions. At the beginning of the simulation, the GDR is similar to the SP strategy because $n_m^k = 0$ for all nodes. The load distributions with $t = 1$ are similar with SP. As the simulation proceeds, the node queue length changes and the GDR strategy starts to take effect. The load distribution starts to change to a Poisson distribution because of the global dynamic information.

Local strategies deliver packets based on the information of neighboring nodes, while the static global strategies only consider the global network topology. GDR takes into account of the intra-layer global and inter-layer coupled dynamic information. The intra-layer information helps to make full use of all link resources, especially links with longer hops but fewer queued packets, to reduce transmission time and improve transmission efficiency. The inter-layer information reduces the use of coupled links and mitigates performance degradation at lower priority layers. The ultimate reason why GDR can achieve simultaneous improvement of multiple transmission metrics and overcome the problems of

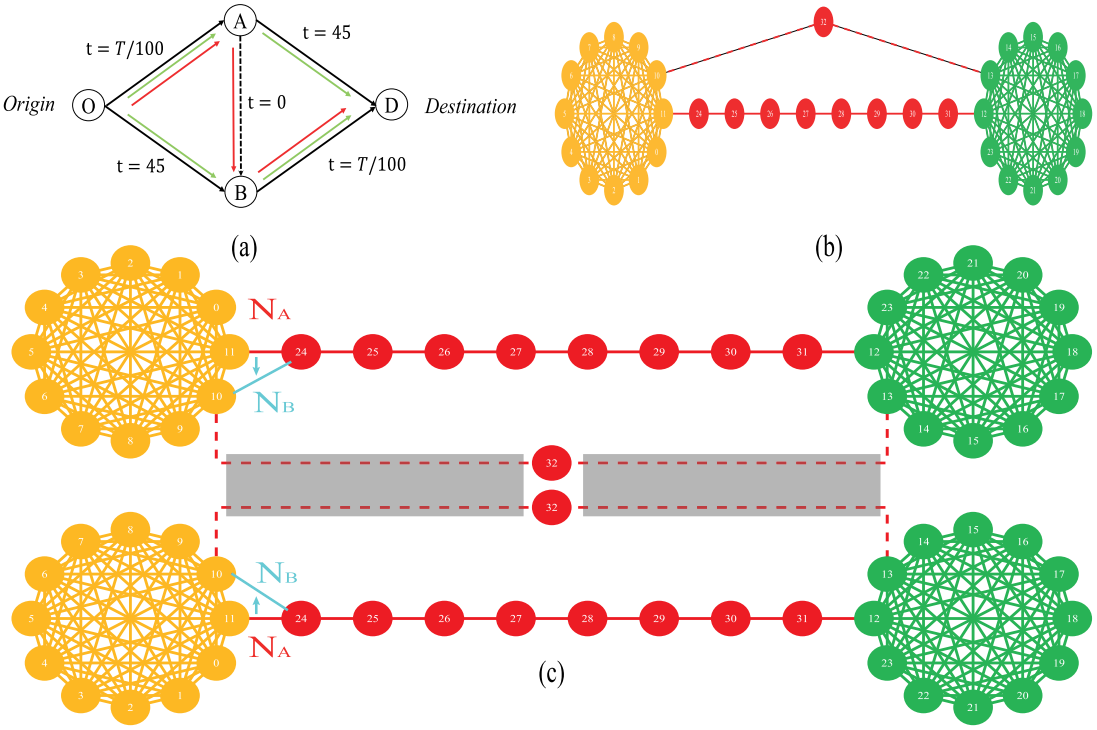


**Fig. 6.** The network topology of Braess's paradox experiment. (a) The classical Braess's paradox case. Drivers start at $O$ and end at $D$. The cost time on $OD(AD)$ always is 45 and the relationship on $OA(BD)$ between the cost time and the packets number is $cost\ time = packets\ numbe/100$. The new link is a di-link from $A$ to $B$, whose cost time is 0. (b) The network topology when $l = 1$. The two fully connected clusters with 12 nodes are connected with a long chain, and the new link is the dashed link. (c) The network topology when $l = 2$. Each layer is the same as the single-layer network. Those new links(dashed links) are coupled with each other. The difference between Network A($N_A$) and Network B($N_B$) is that the link between 11 and 24 is converted to between 10 and 24.

existing strategies in link-coupled networks is the combination of both intra-layer global and inter-layer coupled dynamic information.

## 5. Suppress the occurrence of Braess-like paradox

The classical Braess's paradox network is shown in Fig. 6(a), where there are 4000 drivers from origin to destination. When the directed link $\overrightarrow{AB}$ does not exist, half of drivers choose $O \to A \to D$ and the others choose $O \to B \to D$ with Nash equilibrium. The average time is $2000/100 + 45 = 65$. After adding a new link from $A$ to $B$, all drivers choose $O \to A \to B \to D$, and the average elapsed time is $4000/100 + 45 = 85$. Thus, Braess's paradox occurs because the new link leads to an unfavorable Nash flow ($O \to A \to B \to D$) and longer arrival time.

Braess's paradox can also appear in the link-coupled networks. We give a demonstration of two networks. The networks are shown in Fig. 6(b) and (c). Each packet randomly selects origin and destination among the two fully connected clusters respectively. The difference between $N_A$ and $N_B$ is that the edge of $N_A$ between 11 and 24 is converted to between 10 and 24 at $N_B$. Taking $N_A$ as an example, the packets will be delivered on $O11 \to L0 \cdots L7 \to D11$ with SP strategy. After adding a short chain $O10 \to 32 \to D11$, packets will choose the short chain for transmission. When $l = 2$, since $L_1$ has a higher priority, all packets in $L_2$ are congested. That is, the new short chain provokes serious congestion, similarly to the classical counterintuitive result of Braess' paradox. Although this phenomenon is not the result of self-organizing game theory with SP strategy, it also results in a similar serious congestion like Braess's paradox, thus called Braess-like paradox.

The results of packet transmission on the network are characterized by Arrival Rate ($AR$) and Retention Rate ($RR$, $RR = 1 - AR$). We also analyze the proportion of packets by long links ($LPRA$) and short ($SPRA$, $LPRA + SPRA = AR$) links in the arrival packets, as well as long links ($LPRR$) and short ($SPRR$, $SPRR + LPRR = RR$) links in the retained packets.

In Fig. 7(a), all packets choose short paths for transmission with SP and ER strategy and only half of packets reach the destination. The selfish behavior of each packet leads to the overall performance degradation. In contrast, the packets arriving at the destination select both long and short links evenly with GDR and SGR. In Fig. 7(b), the transmission process of $L_1$ is consistent with that of $l = 1$. All packets in layer $L_2$ select short links for transmission with SP and ER strategy, resulting in $AR = 0$. However, the packets with GDR or SGR select both long and short links evenly, which realizes high AR (Arrival Rate) at Network A ($N_A$). But the reasons for the two strategies are different. Specifically, the reason of GDR

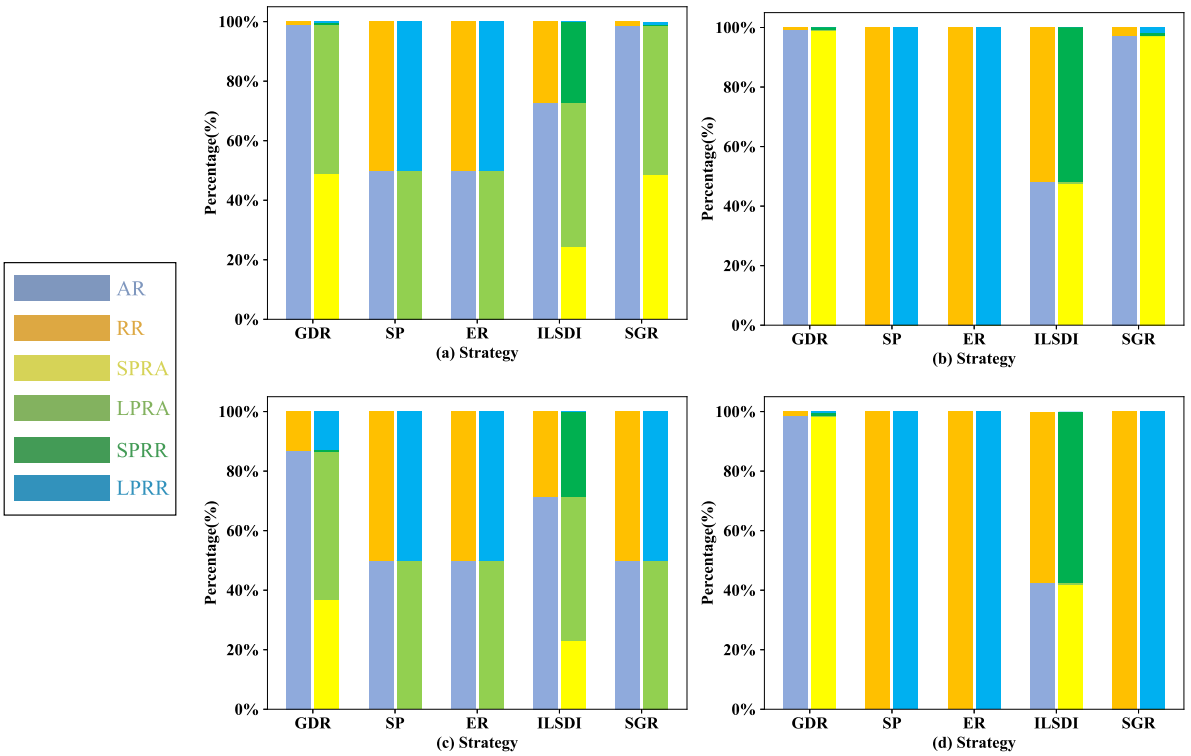


**Fig. 7.** The results of Braess's paradox experiment. We observe the packet arrival rate with different strategies after 1000 time step. The left column represents *AR* and *RR* from bottom to top, and the right column represents *LPRA*, *SPRA*, *SPRR* and *LPRR* from bottom to top. (a) The results with different strategies at $N_A$ when $l = 1$, $R = 2$. (b) The results in $L_2$ with different strategies at $N_A$ when $l = 2$, $R^1 = 2$ (the $R$ in $L_1$) and $R^2 = 1$ (the $R$ in $L_2$). (c) The results with the same conditions as (a) at $N_B$. (d) The results with the same conditions as (b) at $N_B$.

is that the node 32 in $L_1$ is in congestion according to the inter-layer dynamic information. While the reason of SGR is the node 10 in $L_2$ is in congestion according to the intra-layer dynamic information. SGR have been disabled at $N_B$. As shown in Fig. 7(c)(d), SGR performs poorly on $N_B$ and the transmission on $L_2$ is completely congested. The experimental results of other baselines are similar to that on $N_A$. The failure of the SGR is caused by the fact that the node 10 of $L_2$ exists on long and short links at the same time, and the intra-layer dynamic information are not enough to find the proper routing path. However, GDR performs best because of the inter-layer dynamic information. Our work proves that GDR is superior in dealing with link-coupled network by intra-layer and inter-layer global dynamic information and suppresses the occurrence of Braess-like paradox to a certain extent.

## 6. Conclusion

In this paper, we use link-coupled networks to model link-capacity-constrained interconnected networks. We propose a global dynamic routing strategy (GDR) to solve a tradeoff problem of existing strategies on link-coupled networks. Experiments on the link-coupled network demonstrate the excellent performance of GDR from different aspects. Results show that GDR improves various network performance metrics including network capacity, link usage and average arrival time based on the utilization of both intra-layer global and inter-layer coupled dynamic information in Eq. (1). Experiments of Braess's paradox demonstrate that GDR can suppress the Braess-like paradox to a certain extent. We also give an example of congestion without inter-layer dynamic information in our experiments. The introduction of $\delta t$ reduces the time complexity of GDR. It provides the possibility of large-scale use of GDR with an adjustable parameters for transmission rate. The study on load distributions shows the reason why GDR has the highest network capacity and link usage. The evolution of the load distributions of GDR explains the impact of queue length on routing.

GDR extends the global dynamic approach to multi-layer networks, filling a gap in the routing approach on communication networks. The same transport process also exists in power systems and urban transportation systems. Our work can be further applied to the design of transport strategies on these systems.

In the future, we will optimize GDR on more complex networks and explore Braess's paradox on larger real world networks, such as the intermodal bus-and-train transit networks. Since the core transmission resource in link-coupled network is the link capacity, we will use a better resource indicator instead of the length of FIFO queue to represent the congestion state and optimize the transmission.

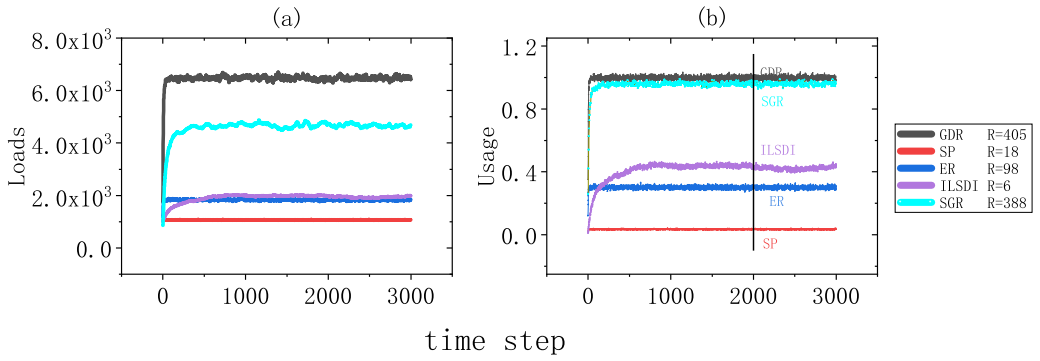


**Fig. 8.** The macro-performance with different strategies. (a) The total number of loads varies with the time step. (b) The link usage varies with the time step.

## CRediT authorship contribution statement

**Chao Yang:** Data curation, Software, Validation, Visualization, Writing – original draft. **Zhuoran Chen:** Validation, Visualization. **Jianghai Qian:** Conceptualization, Methodology, Writing – review & editing. **Dingding Han:** Supervision, Writing – review & editing. **Kaidi Zhao:** Software, Validation, Writing – review & editing.

## Declaration of competing interest

The authors declare that they have no known competing financial interests or personal relationships that could have appeared to influence the work reported in this paper.

## Data availability

No data was used for the research described in the article.

## Acknowledgments

We acknowledge the support of the National Natural Science Foundation of China (Grant nos. 11875133, 12147101 and 11075057) and the Science and Technology Commission of Shanghai Municipality, China (Grant No. 22JC1402500).

## Appendix A. Obtain sampling time and steady state link usage rank

Fig. 8 shows the trend of total load and link usage with time step when $R = 0.9R_c$. When $l = 2$ and $T = 2000$, the system enters steady state. Therefore $t_{sample}$ is set 2000. The order of link usage in steady state is $GDR > SGR > ILSDI > ER > SP$.

## References

[1] M. Kivelä, A. Arenas, M. Barthelemy, J.P. Gleeson, Y. Moreno, M.A. Porter, Multilayer networks, J. Complex Netw. 2 (3) (2014) 203–271.
[2] S. Sreenivasan, R. Cohen, E. López, Z. Toroczkai, H.E. Stanley, Structural bottlenecks for communication in networks, Phys. Rev. E 75 (3) (2007) 036105.
[3] A. Solé-Ribalta, S. Gómez, A. Arenas, Congestion induced by the structure of multiplex networks, Phys. Rev. Lett. 116 (10) (2016) 108701.
[4] H. Youn, M.T. Gastner, H. Jeong, Price of anarchy in transportation networks: efficiency and optimality control, Phys. Rev. Lett. 101 (12) (2008) 128701.
[5] J.E. Cohen, P. Horowitz, Paradoxical behaviour of mechanical and electrical networks, Nature 352 (6337) (1991) 699–701.
[6] A.A. Ganin, M. Kitsak, D. Marchese, J.M. Keisler, T. Seager, I. Linkov, Resilience and efficiency in transportation networks, Sci. Adv. 3 (12) (2017) e1701079.
[7] S. Porta, P. Crucitti, V. Latora, The network analysis of urban streets: a primal approach, Environ. Plan. B: Plann. Des. 33 (5) (2006) 705–725.
[8] I. Kabashkin, J. Kundler, Reliability of sensor nodes in wireless sensor networks of cyber physical systems, Procedia Comput. Sci. 104 (2017) 380–384.
[9] S. Mohebbi, Q. Zhang, E.C. Wells, T. Zhao, H. Nguyen, M. Li, N. Abdel-Mottaleb, S. Uddin, Q. Lu, M.J. Wakhungu, et al., Cyber-physical-social interdependencies and organizational resilience: A review of water, transportation, and cyber infrastructure systems and processes, Sustainable Cities Soc. 62 (2020) 102327.
[10] L. Xu, Q. Guo, H. Sun, Z. Su, A routing optimization model for EMS of power systems considering cyber-physical interdependence, in: 2017 IEEE Conference on Energy Internet and Energy System Integration (EI2), IEEE, 2017, pp. 1–5.
[11] G. Yan, T. Zhou, B. Hu, Z.-Q. Fu, B.-H. Wang, Efficient routing on complex networks, Phys. Rev. E 73 (4) (2006) 046108.

[12] X. Nian, H. Fu, Efficient routing on two layer degree-coupled networks, Phys. A 410 (2014) 421–427.
[13] Y. Bai, D.-D. Han, M. Tang, Multi-priority routing algorithm based on source node importance in complex networks, Internat. J. Modern Phys. C 30 (07) (2019) 1940010.
[14] C.-Y. Yin, B.-H. Wang, W.-X. Wang, T. Zhou, H.-J. Yang, Efficient routing on scale-free networks based on local information, Phys. Lett. A 351 (4–5) (2006) 220–224.
[15] W.-X. Wang, C.-Y. Yin, G. Yan, B.-H. Wang, Integrating local static and dynamic information for routing traffic, Phys. Rev. E 74 (1) (2006) 016101.
[16] W.-X. Wang, B.-H. Wang, C.-Y. Yin, Y.-B. Xie, T. Zhou, Traffic dynamics based on local routing protocol on a scale-free network, Phys. Rev. E 73 (2) (2006) 026111.
[17] B. Danila, Y. Sun, K.E. Bassler, Collectively optimal routing for congested traffic limited by link capacity, Phys. Rev. E 80 (6) (2009) 066116.
[18] X. Ling, M.-B. Hu, W.-B. Du, R. Jiang, Y.-H. Wu, Q.-S. Wu, Bandwidth allocation strategy for traffic systems of scale-free network, Phys. Lett. A 374 (48) (2010) 4825–4830.
[19] A. Asztalos, S. Sreenivasan, B.K. Szymanski, G. Korniss, Distributed flow optimization and cascading effects in weighted complex networks, Eur. Phys. J. B 85 (8) (2012) 1–10.
[20] N.B. Haddou, H. Ez-Zahraouy, A. Rachadi, Implantation of the global dynamic routing scheme in scale-free networks under the shortest path strategy, Phys. Lett. A 380 (33) (2016) 2513–2517.
[21] M. Tang, T. Zhou, Efficient routing strategies in scale-free networks with limited bandwidth, Phys. Rev. E 84 (2) (2011) 026116.
[22] M.-B. Hu, W.-X. Wang, R. Jiang, Q.-S. Wu, Y.-H. Wu, The effect of bandwidth in scale-free network traffic, Europhys. Lett. 79 (1) (2007) 14003.
[23] D.-H. Kim, A.E. Motter, Resource allocation pattern in infrastructure networks, J. Phys. A 41 (22) (2008) 224019.
[24] M. Li, M.-B. Hu, B.-H. Wang, Transportation dynamics on coupled networks with limited bandwidth, Sci. Rep. 6 (1) (2016) 1–8.
[25] L. Kang, H. Li, H. Sun, J. Wu, Z. Cao, N. Buhigiro, First train timetabling and bus service bridging in intermodal bus-and-train transit networks, Transp. Res. B 149 (2021) 443–462.
[26] L. Kang, H. Sun, J. Wu, Z. Gao, Last train station-skipping, transfer-accessible and energy-efficient scheduling in subway networks, Energy 206 (2020) 118127.
[27] University of California's San Diego Supercomputer Center, Macroscopic internet topology data kit (ITDK) - CAIDA, 2022, https://www.caida.org/catalog/datasets/internet-topology-data-kit/.
[28] X. Ling, M.B. Hu, R. Jiang, Q.S. Wu, Global dynamic routing for scale-free networks, Phys. Rev. E 81 (1) (2010) 016113.
[29] Y. Hu, M. Xu, M. Tang, D. Han, Y. Liu, Efficient traffic-aware routing strategy on multilayer networks, Commun. Nonlinear Sci. Numer. Simul. 98 (2021) 105758.
[30] D. Braess, Über ein paradoxon aus der verkehrsplanung, Unternehmensforschung 12 (1) (1968) 258–268.
[31] S. Manfredi, E. Di Tucci, V. Latora, Mobility and congestion in dynamical multilayer networks with finite storage capacity, Phys. Rev. Lett. 120 (6) (2018) 068301.
[32] A. Rapoport, T. Kugler, S. Dugar, E.J. Gisches, Choice of routes in congested traffic networks: Experimental tests of the braess paradox, Games Econom. Behav. 65 (2) (2009) 538–571.
[33] S. Bittihn, A. Schadschneider, The effect of modern traffic information on Braess' paradox, Phys. A 571 (2021) 125829.
[34] D. Easley, J. Kleinberg, et al., Networks, crowds, and markets: Reasoning about a highly connected world, Significance 9 (1) (2012) 245–253.
[35] G. Valiant, T. Roughgarden, Braess's paradox in large random graphs, Random Struct. Algorithms 37 (4) (2010) 495–515.
[36] F. Chung, S.J. Young, Braess's paradox in large sparse graphs, in: International Workshop on Internet and Network Economics, Springer, 2010, pp. 194–208.
[37] A. Arenas, A. Díaz-Guilera, R. Guimera, Communication in networks with hierarchical branching, Phys. Rev. Lett. 86 (14) (2001) 3196.